

This discussion paper is/has been under review for the journal Hydrology and Earth System Sciences (HESS). Please refer to the corresponding final paper in HESS if available.

Applicability of ensemble pattern scaling method on precipitation intensity indices at regional scale

Y. Li¹ and W. Ye²

¹Climsystems Ltd. Hamilton, 3240, New Zealand

²The University of Waikato, Hamilton, 3240, New Zealand

Received: 10 May 2011 – Accepted: 18 May 2011 – Published: 26 May 2011

Correspondence to: Y. Li (yinpengli@climsystems.com)

Published by Copernicus Publications on behalf of the European Geosciences Union.

HESSD

8, 5227–5261, 2011

Applicability of ensemble pattern scaling method

Y. Li and W. Ye

Title Page

Abstract

Introduction

Conclusions

References

Tables

Figures

◀

▶

◀

▶

Back

Close

Full Screen / Esc

Printer-friendly Version

Interactive Discussion



Abstract

Pattern scaling constructs future climate change scenarios using the normalized change patterns of GCMs, offers the possibility of representing the whole range of uncertainties involved in future climate change projection. This paper investigates the applicability and uncertainty associated with the pattern scaling method in constructing the changes of future precipitation intensity indices at regional scale, using a two-step ensemble approach. In the first step, the linearity accuracy and GCM internal variability were examined explicitly. The inter-model variability of the GCMs and associated confidence intervals were produced in the second step ensemble. Australia and its 7 administrative regions was selected as the study area and three precipitation intensity indices, including two precipitation extreme indices, were used for the examination: i.e., the 99th percentile daily precipitation intensity (P_{99}), the 20-yr-return extreme precipitation intensity (RP_{20}), and the mean precipitation intensity (precipitation amount per wet day) (RPD). A total of 12 IPCC AR4 GCMs with 6 simulation samples were used for the ensemble. For the 3 precipitation intensity indices, good linear relationships between precipitation intensity indices change and global mean temperature change at the national level were found for most GCMs, however, the linear relationship weakened when the analysis was applied to the administrative regions. In addition, the GCM internal signal-to-noise ratios for each GCM tended to decrease at the regional and grid cell levels, along with the reduction in spatial scale. Both GCM-internal and inter-model variability was significant, and the inter-model variability was larger than GCM-internal variability. The final result of the inter-model ensemble median results show that for Australia, in general, all three indices will increase under global warming, with the change rates being 3.56, 7.62 and 2.26 % K^{-1} for P_{99} , RP_{20} and RPD respectively at the national level.

HESSD

8, 5227–5261, 2011

Applicability of ensemble pattern scaling method

Y. Li and W. Ye

Title Page

Abstract

Introduction

Conclusions

References

Tables

Figures

◀

▶

◀

▶

Back

Close

Full Screen / Esc

Printer-friendly Version

Interactive Discussion



1 Introduction

While it is generally agreed that General Circulation Models (GCMs) are still the best tools in constructing future climate change scenarios, the large variation of simulation result from different GCM runs, or even from the same GCM but with different radiative forcing, has caused great difficulty in applying the GCM result directly in climate impact analysis when the range of uncertainties become an important factor in adaptation planning consideration. Since early 1990s, an alternative method has been developed in constructing future climate change scenarios instead of using GCM outputs directly (Santer et al., 1990). Such a method, known as pattern scaling, was originally envisaged as a temporary compromise to add a time component to an equilibrium experiment with a GCM, pending the availability of transient experiments, and also to permit the comparison of standardised spatial patterns from different GCMs (Santer et al., 1990). However, this technique has been proved to be very useful for a comprehensive risk assessment of climate change when more and more GCM outputs have become publicly available (Mitchell, 2003; Li et al., 2009). Pattern scaling offers the possibility of representing the whole range of uncertainties involved in future climate change projections based on various combinations of emission scenarios and GCM outputs, which allows cross model sensitivity analyses and uncertainty examinations to be conducted easily (TGICA, 2007). It has been widely used in mean temperature and precipitation change studies (Mitchell, 2003; Ruosteenoja et al., 2007).

Pattern scaling is based on the theory that, firstly, a simple climate model can accurately represent the global responses of a GCM, even when the response is non-linear (Raper et al., 2001), and secondly, a wide range of climatic variables represented by a GCM are a linear function of the global annual mean temperature change represented by the same GCM at different spatial and/or temporal scales (Mitchell, 2003). Pattern-scaling does not seem to be a very large source of error in constructing regional climate projections for extreme scenarios (Ruosteenoja et al., 2007), however, in applying pattern-scaling, two fundamental sources of error related to its underlying theory need to be addressed: (1) Nonlinearity error: the local responses of climate

Applicability of ensemble pattern scaling method

Y. Li and W. Ye

Title Page

Abstract

Introduction

Conclusions

References

Tables

Figures



Back

Close

Full Screen / Esc

Printer-friendly Version

Interactive Discussion



variables, precipitation in particular, may not be inherently linear functions of the global mean temperature change; and (2) Noise due to the internal variability of the GCM.

Among the wide range of climate variables, precipitation extremes have attracted much research attention because of the potential disasters these may cause to human society and natural systems. Extreme precipitation events are projected to increase with climate change, even in areas where the total precipitation is projected to decrease (Meehl et al., 2007), since global warming will noticeably enhance the hydrological cycle at both global and local scales. In order to adequately assess the climate change impact on extreme precipitation events, the characteristics of GCM-simulated precipitation and its relationship with global warming need to be evaluated (Perkins et al., 2007; Alexandra and Arblaster, 2008). The evaluation of observed and modeled trends has shown that the confidence in GCM projected extremes of precipitation is much less than that of temperature (e.g. Kharin et al., 2007; Kiktev et al., 2007). In general, the magnitude of changes in precipitation extremes simulated by GCMs was found to have a linear relationship with the strength of GHG emissions or in proportion with the global warming trend (Alexander and Arblaster, 2009; Tebaldi et al., 2006), which is inline with the linear response theory of pattern scaling.

On the other hand, given the current state of scientific understanding and the limitations of GCMs in simulating the complex climate system, a large ensemble of GCM simulations is more appropriate in climate change projections than using individual GCM simulation outputs, particularly if such projections will be used for impact assessments, because only large ensemble of GCM simulations sampling the widest possible range of modelling uncertainties can provide a reliable specification of the spread of possible regional changes (Murphy et al., 2004, 2007; Sorteberg and Kvamsto, 2006; Räisänen, 2007). With respect to using the ensemble approach for inter-model uncertainty analysis, several methods have been introduced from past studies. The Reliability Ensemble Average (REA) method (Giorgi and Mearns, 2002) quantifies two criteria, bias and convergence, for multi-model evaluation, and produces estimates of regional climate change, the associated uncertainty bounds and model reliabilities through a

Applicability of ensemble pattern scaling method

Y. Li and W. Ye

Title Page

Abstract

Introduction

Conclusions

References

Tables

Figures



Back

Close

Full Screen / Esc

Printer-friendly Version

Interactive Discussion



weighted average of the individual GCM results. The REA weights contain a measure of model bias with respect to current climate and a measure of model convergence (applied to the models' projected change), defined as the deviation of the individual projection with respect to the central tendency of the ensemble (i.e., the final weighted average). Another method of multi-model ensemble in probabilistic climate projections is the Bayesian approach (Tebaldi et al., 2005; Ferrer et al., 2007). The premise of this method is that outliers are likely to be less credible and would lead to over-dispersive uncertainty estimates if included. This issue is inevitably open to debate, but it is clear that probabilistic estimates derived from multi-model ensembles are significantly dependent on methodological choices necessitated by the nature of the ensembles (Lopez et al., 2006).

Simulations of extreme precipitation in GCMs cannot be expected to accurately reproduce observed absolute quantities or rates of change. The relatively coarse resolution of GCMs prevents the simulation of phenomena that manifest their intensity mainly at synoptic scales (Dai, 2006; Tebaldi et al., 2006). GCM simulated extreme precipitation intensities are systemically much lower than the observed data (Dai, 2006; Kharin et al., 2007), therefore, skill based weighting ensemble method, such as REA or Bayesian model averaging (Min et al., 2007) are not applicable for precipitation intensity change predictions for this research.

In this paper we present a two-step ensemble method to test the applicability of pattern scaling in constructing the future change of precipitation intensity indices and the associated uncertainties. In the first step ensemble, the linearity accuracy and GCM internal variability were examined. The GCMs inter-model variability with confidence intervals was produced in the second step ensemble. Australia and its 7 administrative regions were selected as the study area and three precipitation intensity indices, including two precipitation extreme indices, were used for the examination, i.e.: the 99th percentile daily precipitation intensity (P_{99}), the 20-yr-return extreme precipitation intensity (RP_{20}), and the mean precipitation intensity (precipitation amount per wet day) (RPD).

Applicability of ensemble pattern scaling method

Y. Li and W. Ye

Title Page

Abstract

Introduction

Conclusions

References

Tables

Figures

◀

▶

◀

▶

Back

Close

Full Screen / Esc

Printer-friendly Version

Interactive Discussion



Based on the data availability, a total of 12 IPCC AR4 GCMs were selected for this study. They are labeled as GCM 1 to 12 in this paper, following the sequence of: 1 – BCCR_BCM20; 2 – CCCMA_CGM3(T47); 3 – CNRM_CM3; 4 – CSIRO MK35; 5 – ECHAM_MPI; 6 – ECHO_G; 7 – GFDL_CM20; 8 – GFDL_CM21; 9 – IPSL_CM40; 10 – MIROC_MEDRES; 11 – MRI_CGCM2; 12 – NCAR_CCSM3. All GCM daily precipitation and monthly mean temperature data were obtained from the WCRP CMIP3 multi-model dataset (<https://esg.llnl.gov:8443/>).

2 Methodology and data

The two step ensemble method included a GCM-internal ensemble and an inter-model ensemble. A linear least square regression line fitting method described by Mitchell et al. (2003) and Ruosteenoja et al. (2007) was employed for the GCM-internal ensemble in this research. Based on the pattern scaling theory, for a given GCM, the linear response change pattern of a climate variable to global mean temperature change represented by the GCM, should be obtained from any one of its GHG emission simulation outputs. However, such a consistent linear response is rarely found from the outputs of a given GCM running under different radiative forcings, or for the same radiative forcing but different simulation periods. The reason is partly due to our limited understanding of the climate system, and partly due to the randomness of the climate variation in the GCM simulations. Hence the objective of the first step ensemble is to reduce the impact of the GCM internal variability from the sampled emission scenarios and time periods.

Pattern scaling may be described as follows: for a given climate variable V , its anomaly ΔV^* for a particular grid cell (i), month or season (j) and year or period (y) under an emission forcing scenario (x):

$$\Delta V_{xyij}^* = \Delta T_{xy} \cdot \Delta V'_{ij} \quad (1)$$

ΔT being the annual global mean temperature change.

Applicability of ensemble pattern scaling method

Y. Li and W. Ye

Title Page

Abstract

Introduction

Conclusions

References

Tables

Figures

◀

▶

◀

▶

Back

Close

Full Screen / Esc

Printer-friendly Version

Interactive Discussion



The ensemble pattern value ($\Delta V'_{ij}$) was calculated from the GCM simulation anomaly (ΔV_{xyij}) using linear least squares regression, that is, the slope of the fitted linear line.

$$\Delta V'_{ij} = \frac{\sum_{y=1}^m \sum_{x=1}^n \Delta T_{xy} \cdot \Delta V_{xyij}}{\sum_{y=1}^m \sum_{x=1}^n (\Delta T_{xy})^2} \quad (2)$$

where n is the number of emission scenarios and m is the number of future sample periods used. The size of the GCM-internal ensemble was $m \times n$. In this research, three SRES scenarios (A1B, A2, and B1) and 2 sample periods (2046–2065 and 2081–2100) were used. Therefore, the ensemble size was 6 as there were 6 simulation samples for each of the 12 GCMs. For a given climate variable, its regional change patterns of per degree global warming were calculated by applying Eq. (2) for each GCM, and the GCM-internal standard deviation (SD) was calculated based on its 6 simulation samples. A signal-to-noise ratio (SNR) was used to reveal the significance level of a climate variable to noise that included in simulations:

$$\text{SNR} = \frac{|\Delta V'|}{\text{SD}(\Delta V')} \quad (3)$$

In the inter-model ensemble step, the median (50th percentile) value was used in presenting the average ensemble result, which is arguably better than the mean value (Kharin et al., 2007), while the 10th and 90th percentiles were used for the confidence intervals analysis, or to demonstrate the range of uncertainties from different GCM simulations. The confidence intervals were computed with a bootstrapping approach (Chernick, 1999). We assumed that the change rate generated from GCMs fitted with a generalized Weibull distribution. The L -moments method (Hosking, 1992) was firstly applied in estimating the parameters of the generalized Weibull distribution. Then the bootstrap mean for a specified confidence interval was generated from 400

Applicability of ensemble pattern scaling method

Y. Li and W. Ye

Title Page

Abstract

Introduction

Conclusions

References

Tables

Figures

◀

▶

◀

▶

Back

Close

Full Screen / Esc

Printer-friendly Version

Interactive Discussion



random re-sampling simulations. More detailed descriptions on the application of L -moment and bootstrapping methods can be found in Kharin et al. (2007) and Tebaldi et al. (2006). All three precipitation intensity indices were calculated from IPCC AR4 GCM daily precipitation outputs for three SRES scenarios (A1B, A2, and B1) and 2 future periods (2046–2065 and 2081–2100). The period of 1981–2000 was used to represent the baseline condition as suggested by IPCC AR4 (IPCC, 2007). The 99th percentile precipitation intensity (P_{99}) was estimated using the non-parameter Gauss kernel density method (Parzen, 1962). The 20-yr return daily precipitation intensity (RP_{20}) was calculated from the General Extreme Value (GEV) distribution using the L -moments parameter estimation (Hosking, 1992). The mean precipitation intensity (RPD) was calculated as the total precipitation amount divided by the number of wet days (precipitation >1 mm). Once the intensity indices were calculated for each grid cell, their simulation anomaly were calculated by comparing the difference between future projections and the baseline, and then the ensemble pattern values were calculated using Eq. (2).

3 Results

3.1 The 99th percentile daily precipitation intensity changes

3.1.1 The linearity of the 99th percentile daily precipitation intensity change (ΔP_{99}) in response to global annual mean temperature change (ΔT).

Figure 1 shows the linearity of ΔP_{99} in response to ΔT of the 12 GCMs at national scale. Also shown in the figure is the R^2 . A value of R^2 higher than 0.6577 correlation coefficient, $r > 0.811$, $n - 2 = 4$ indicates the linear relationship passed the 95 % significance level. Among the 12 GCMs, 8 GCMs had R^2 values that passed the 95 % significance level, which showed a strong linear response of ΔP_{99} to ΔT . Three GCMs, BCCR_BCM20, MRI_CGCM2 and NCAR_CCSM3, have small R^2 values, showing that

Applicability of ensemble pattern scaling method

Y. Li and W. Ye

Title Page

Abstract

Introduction

Conclusions

References

Tables

Figures

◀

▶

◀

▶

Back

Close

Full Screen / Esc

Printer-friendly Version

Interactive Discussion



almost no linearity could be detected from these 3 models. CSIRO_MK35 demonstrated reasonable linearity between ΔP_{99} and ΔT , as indicated by its moderate R^2 values. GFDL_CM20 had the most rapid change with increased rates exceeding $10\%K^{-1}$ by all its 6 simulations. The lowest change rate was found in NCAR_CCSM3, which had all 6 simulations of less than $1\%K^{-1}$. A negative sign in ΔP_{99} against ΔT was found in BCCR_BCM20 in its A1B 2046–2065 simulation, while the change rates from its other 5 simulations were all positive.

Though most of the GCMs demonstrated a high level of linearity of ΔP_{99} against ΔT at the national scale, such a good linearity was not found at the regional level. Table 1 lists the R^2 of each GCM for the 7 administrative regions. Compared to 8 GCMs at national level, there were 3 to 5 GCMs that passed the 95% significance level for the linearity test for each administrative region. NSW, TAS, and VIC all had 5 GCMs, while NT and QLD only had 3 GCMs. For each GCM, normally 2 to 4 regions showed significant linear correlations, except BCCR_BCM20 with no region having significant linear correlation between ΔP_{99} and ΔT . For CSIRO_MK35 and NCAR_CCSM3, their linear correlations were not significant at the national scale, but passed the 95% significance level in 2 regions.

3.1.2 The comparison of GCM-internal and inter-model variability of the 99th percentile daily precipitation intensity change

For each GCM, also listed in Table 1 is the ensemble pattern values ($\Delta P'_{99}$) and its signal-to-noise ratio (SNR) calculated from the 6 samples for Australia and its 7 administrative regions. ECHAM_MPI, ECHO_G and MIROC_MEDRES showed moderate to high increase rates (from 6.91 to $10.86\%K^{-1}$ for ECHAM_MPI, 2.42 to $8.86\%K^{-1}$ for ECHO_G and 2.06 to $10.12\%K^{-1}$ for MIROC_MEDRES) and most importantly with relative strong signals for all regions (SNR from 2.27 to 6.61 for ECHAM_MPI, 2.24 to 6.48 for ECHO_G and 1.72–4.27 for MIROC_MEDRES). Most regions simulated by CNRM_CM3, CSIRO_MK35, GFDL_CM20, GFDL_CM21 and IPSL_CM40 that had high change rates were also accompanied with relatively strong signals.

Applicability of ensemble pattern scaling method

Y. Li and W. Ye

Title Page

Abstract

Introduction

Conclusions

References

Tables

Figures

◀

▶

◀

▶

Back

Close

Full Screen / Esc

Printer-friendly Version

Interactive Discussion



Applicability of ensemble pattern scaling method

Y. Li and W. Ye

Title Page

Abstract

Introduction

Conclusions

References

Tables

Figures

◀

▶

◀

▶

Back

Close

Full Screen / Esc

Printer-friendly Version

Interactive Discussion



For some models, the $\Delta P'_{99}$ varied significantly from one region to another, GFDL_CM21 in particular with its $\Delta P'_{99}$ range from 0.86 to 15.11 %K⁻¹, which indicated the significant spatial difference of $\Delta P'_{99}$ in response to ΔT . Furthermore, $\Delta P'_{99}$ could vary significantly from one GCM to another for the same region. For example, NT had a $\Delta P'_{99}$ range from -1.17 to 24.72 %K⁻¹. The range was reduced at the national level, changing from 0.82 to 13.77 %K⁻¹ but was still significant.

Figure 2 illustrates the GCM internal and inter-model variability in annual $\Delta P'_{99}$ over Australia. For each GCM, the 6 sample values were distributed randomly, independent of both the emission scenarios and the time period. BCCR_BCM20 and ISPL_CM40 showed the largest SD among GCMs (shown in Fig. 1), because of the unusual result from one sample of its simulation. GFDL_CM21 also showed a larger SD with a large increase rate of $\Delta P'_{99}$. Both MRI_CGCM2 and NCAR_CCSM3 had small SDs with no increase rates, however, the respective R^2 values did not pass the 95 % significant level test. The inter-model SD was 7.23 (shown in Table 5), therefore much larger than any one of the GCM internal SD, which was also shown in Fig. 2 as the relative short bars compared to the wide range of $\Delta P'_{99}$ values from the 12 GCMs.

3.2 The 20-yr return daily precipitation intensity changes

3.2.1 The linearity of the 20-yr return period precipitation intensity change (ΔRP_{20}) in response to global annual mean temperature change (ΔT)

Figure 3 shows the linearity of ΔRP_{20} in response to ΔT and the R^2 of the 12 GCMs for Australia. Among them, six of the GCMs passed the 95 % linearity significance level with R^2 values larger than 0.6577, showing strong linearity signals were detected by these models. Almost no linearity signal could be detected from the MIROC_MEDRES and NCAR_CCSM3 models. The remaining 4 models, BCCR_BCM20, CNRM_CM3, CSIRO MK35 and MRI_CGCM2 showed some linearity signals, with their R^2 range from 0.32 to 0.44.

Similar to ΔP_{99} , at the regional level, the significance of the linearity between ΔRP_{20} and ΔT decreased compared to the national scale, as shown by the R^2 for each region in Table 2. For most regions, there were 2 to 5 GCMs that pass 95 % significant level test, including 5 GCMs for VIC, 2 GCMs for QLD, much less than for the overall Australian area. Among the GCMs where the correlation coefficients did not pass the 95 % significant level at the national level, MIROC_MEDRES and NCAR_CCSM3 had one region each that did pass the 95 % significant level.

3.2.2 The comparison of GCM internal and inter-model variability of the 20-yr return period precipitation intensity change

For each GCM, Table 2 also lists the ensemble pattern values for the 20-yr return period precipitation intensity change ($\Delta RP'_{20}$) and its SNR calculated from 6 simulation samples for Australia and its administrative regions. In general, the 6 models that had good linearity signals at the national level also had high SNR for most regions. IPSL_CM40 showed a negative $\Delta RP'_{20}$ ($-0.23\%K^{-1}$) for VIC but with a very small SNR (0.06). GFDL_CM20, GFDL_CM21, and CCCMA_CGM3 (T47) showed a relatively high increase rate of $\Delta RP'_{20}$ for most regions, even though there was large variability between regions. MRI_CGCM2, NCAR_CCSM3 had poor SNR for almost all regions, while other models had varied SNR for different regions. Again, for the same region, the $\Delta RP'_{20}$ varied significantly from one GCM to another, NT in particular had a $\Delta RP'_{20}$ ranging from 0.97 to $36.87\%K^{-1}$. The range was reduced at the national level, from 2.21 to $20.40\%K^{-1}$.

Figure 4 gives the GCM internal and inter-model variability in annual $\Delta RP'_{20}$ over Australia. For each GCM, the 6 sample values were distributed randomly, similar to that of ΔP_{99} . Compared with ΔP_{99} , the SD values of $\Delta RP'_{20}$ were larger. IPSL_CM40, CCCMA_CGCM3 and MRI_CGCM2 showed the largest SD among GCMs. GFDL_CM21 also showed a larger SD with a large increase rate of $\Delta RP'_{20}$, similar to its performance in $\Delta P'_{99}$. CSIRO_MK35 had relatively smaller SD, however, its R^2 did not pass

Applicability of ensemble pattern scaling method

Y. Li and W. Ye

Title Page

Abstract

Introduction

Conclusions

References

Tables

Figures



Back

Close

Full Screen / Esc

Printer-friendly Version

Interactive Discussion



the 95 % significance level test. Only ECHO_G gave both higher R^2 and lower SD. The inter-model SD of $\Delta RP'_{20}$ was $9.36 \%K^{-1}$ (shown in Table 5), which was the largest among all the GCM internal SD values.

3.3 The mean daily precipitation intensity changes

3.3.1 The linearity of the mean daily precipitation intensity change (ΔRPD) in response to global annual mean temperature change (ΔT)

At national scale, Fig. 5 shows the linearity of the change of mean daily precipitation intensity (ΔRPD) in response to ΔT for the 12 GCMs. Nine GCMs showed a strong signal of linear response of ΔRPD to global mean temperature change, with R^2 values higher than the 95 % significance level. CSIRO_MK35 and MRI_CGCM2 showed no linearity signals, while BCCR_BCM20, GFDL_CM21 and MIROC_MEDRES show some linearity signals (R^2 are 0.68, 0.40 and 0.69 respectively). ECHAM_MPI shows the most rapid change and the lowest change rate is found in CSIRO_MK35.

The R^2 values of ΔRPD for each region and each GCM are shown in Table 3. In each region, there were 2 to 7 GCMs passed the 95 % significance level test, which was less than the 9 GCMs at the national level for Australia. In VIC, 7 GCMs passed 95 % significant level test, while in QLD 2 GCMs passed. Among GCMs which showed a significant correlation between ΔRPD and ΔT for Australia, there were 0 to 6 regions which showed significant correlations. For IPSL_CM40 the national correlation coefficient passed the 95 % significance level test, but no region in Australia passed the test. For ECHAM_MPI, 6 regions passed the test with some high R^2 values. Noticeable, for NCAR_CCSM3, the overall R^2 of ΔRP_D is 0.92 and 5 regions also passed the 95 % significance level test, however, in ΔRP_{20} and ΔP_{99} no significant correlations were detected. Among the GCMs for which the correlation coefficients did not pass the 95 % significance level, GFDL_CM21 had one region which did pass the 95 % significance level. The ΔRPD had the best performance, in terms of the linear relationship with ΔT , among the three precipitation intensity indices.

Applicability of ensemble pattern scaling method

Y. Li and W. Ye

Title Page

Abstract

Introduction

Conclusions

References

Tables

Figures



Back

Close

Full Screen / Esc

Printer-friendly Version

Interactive Discussion



3.3.2 GCM internal variability of the mean daily precipitation intensity change

For each GCM, Table 3 lists the ensemble pattern values ($\Delta\text{RPD}'$) and its SNR calculated from 6 simulation samples for Australia and its 7 administrative regions. The 9 models that had good linearity performance at the national level also showed reasonably high SNR for most regions, except GFDL_CM20 that had small SNR for 4 out of the 7 regions. In general, the 3 GCMs that showed some linearity signals (BCCR_BCM20, GFDL_CM21 and MIROC_MEDRES) all had reasonable SNR. As shown in Table 3, the internal variability was small across regions compared to $\Delta P'_{99}$ and $\Delta\text{RP}'_{20}$, which indicated relatively consistent projections of $\Delta\text{RPD}'$ from all GCMs. ECHAM_MPI had relatively high $\Delta\text{RPD}'$ for all regions except TAS; and IPSL_CM40 had the largest range of $\Delta\text{RPD}'$ across the country (from -1.94 to $4.22\%K^{-1}$). A few models projected decreased $\Delta\text{RPD}'$ for some regions shown by the negative numbers in Table 3. For the same regions, the $\Delta\text{RPD}'$ varied from one GCM to another, but with a smaller range compared to $\Delta P'_{99}$ and $\Delta\text{RP}'_{20}$. The $\Delta\text{RPD}'$ range was 1.49 to $5.19\%K^{-1}$ at the national level for the 10 models that showed moderate to good linearity.

The variations of $\Delta\text{RPD}'$ were generally smaller than the other two indices (Fig. 6). MRI_CGCM2 had the largest SD (2.4), while others were less than 1.0. NCAR_CCSM and ECHO_G had the smallest SD with high R^2 . Negative $\Delta\text{RPD}'$ values appeared in several simulations of CSIRO_MK35 and MRI_CGCM2. The inter-model SD for $\Delta\text{RPD}'$ was 2.41, which was larger than the GCM internal SDs over Australia.

3.4 Comparison of the grid cell to grid cell signal-to-noise ratios (SNR)

Further studies were carried out at the grid-cell ($0.25^{\circ} \times 0.25^{\circ}$ degree) scale to investigate the spatial pattern of signal-to-noise ratios of the three indices. A larger percentage of high SNR at the grid cell level, represented a more consistent result from different simulation samples of a GCM. For each GCM, we analysed the SNR level of 0.5, 1.0 and 2.0 based on grid cell, and the statistical results are displayed in Table 4.

Applicability of ensemble pattern scaling method

Y. Li and W. Ye

Title Page

Abstract

Introduction

Conclusions

References

Tables

Figures



Back

Close

Full Screen / Esc

Printer-friendly Version

Interactive Discussion



Applicability of ensemble pattern scaling method

Y. Li and W. Ye

Title Page

Abstract

Introduction

Conclusions

References

Tables

Figures

◀

▶

◀

▶

Back

Close

Full Screen / Esc

Printer-friendly Version

Interactive Discussion



For $\Delta P'_{99}$, the average SNR for all GCMs showed that more than 80 % of the grid cells had values larger than 0.5, about half larger than 1.0, and a little over 10 % larger than 2.0. Among the GCMs, ECHAM_MPI had the best performance, followed by ECHO_G and MIROC_MEDRES. More than 20 % of the grid cells of the above GCMs had their SNR greater than 2.0. Four GCMs, i.e., BCCR_BCM20, MRI_CGCM2, NCAR_CCSM3 and GDFL_CM21, had less than 10 % of the grid-cells with a SNR larger than 2.0 and less than 50 % grid cell SNR larger than 1.0, and BCCR_BCM20 had the lowest values in all three SNR levels of the GCMs.

Compared to $\Delta P'_{99}$, a small improvement was shown in the grid cell SNR level of $\Delta RP'_{20}$. On average, nearly 90 % grid cells had values larger than 0.5, more than half passed 1.0, and about 17 % passed 2.0. This improvement was the result of increased SNR values for most GCMs. However, 2 GCMs showed worse SNR performance than for $\Delta P'_{99}$ (these were CSIRO_MK35 and MIROC_MEDRES).

The $\Delta RP'D'$ had the highest SNR levels among the three indices. Four GCMs had more than half of the grid cells that show strong signals with SNR greater than 2.0. In contrast to its performance of $\Delta P'_{99}$ and $\Delta RP'_{20}$, NCAR_CCSM3 had a high level of SNR with 55.26 % of its grid cells greater than 2.0. ECHO_G and ECHAM5_MPI had the best values, similar to their performance in the other 2 indices. On average, more than 60 % grid cells had SNR higher than 1.0 and about a third had SNR close to 2.0.

The spatial patterns of these SNRs can be found in the Supplementary Fig. 1 to supplementary Fig. 3

3.5 Inter-model ensemble

Inter-model variability is one of the major sources of uncertainty for future climate projection. As demonstrated in the previous sections, for the same region the change pattern of precipitation indices can vary significantly among GCM simulations, usually much larger than any GCM-internal variability from pattern scaling. As a result of such high uncertainties, a large ensemble of GCM predictions sampling the widest possible

modelling range are needed to understand the range of uncertainties due to different GCM results and to have such uncertainties properly analyzed in subsequent impact assessments.

For the three precipitation indices, we carried out an inter-model ensemble based on the 12 GCMs. The first step of the ensemble was to generate the normalised climate change pattern value $\Delta V'$ for each grid cell, which was calculated from the 6 samples (3 SRES scenarios by 2 sample periods) for each GCM. The second step was to apply the bootstrap method to obtain the median, as well as the 10th and 90th percentiles of $\Delta V'$ for each grid cell based on the 12 GCM projections. Figure 7 shows the spatial distributions of the median and SD of the $\Delta P'_{99}$, $\Delta RP'_{20}$ and $\Delta RPD'$ from the ensemble. It showed that the change rates of the 3 indices all increased under global warming, as $\Delta P'_{99}$ and $\Delta RPD'$ had positive median values for most of the country, while the median values of $\Delta RP'_{20}$ were positive for the entire country. In general, southeast regions (NSW, SA, TAS, and VIC) had lower SD than the north and west regions (NT, QLD and WA), which meant a smaller inter-model variability in the southeast (Fig. 7). VIC had the highest change rates for both P_{99} and RPD among regions, also with relatively small SD, indicating a consistent projection of high ΔP_{99} and ΔRPD change rates from all GCMs for VIC. The boarder between QLD and NT was another area that had the high change rate for all 3 indices, but was accompanied with relatively high SD, which meant relatively high inter-model uncertainties.

To reveal the statistical nature of the uncertainties in the ensemble results, we aggregated their median value to regional and national levels, then, calculated the averages. Table 5 lists the average median value results for Australia and its administrative regions, as well as the inter-modal standard deviation (SD) and the 10th, 90th percentiles. At the regional average, the median values of the 3 indices were all positive, indicating enhanced precipitation extremes for the whole country for this century. Most of the 10th percentiles for the 3 indices are around zero, which means that 10% of GCMs simulated change rates which were not significant. On the other hand, another 10% of GCMs demonstrate a dramatically increased change rates, shown by the large

Applicability of ensemble pattern scaling method

Y. Li and W. Ye

Title Page

Abstract

Introduction

Conclusions

References

Tables

Figures

◀

▶

◀

▶

Back

Close

Full Screen / Esc

Printer-friendly Version

Interactive Discussion



change values of the 90th percentiles. VIC had the highest average median values for $\Delta P'_{99}$, and $\Delta RPD'$, which was consistent with Fig. 7.

As summarized in Table 5, the annual median value of $\Delta P'_{99}$ at the national level for Australia was $3.56 \% K^{-1}$, with significant inter-model standard deviations ($7.23 \% K^{-1}$).

Most of the 10th percentile $\Delta P'_{99}$ values were negative, except for TAS, while most of the 90th percentile values ranged from 10 – $20 \% K^{-1}$. The median value of annual $\Delta RP'_{20}$ over Australia was $7.62 \% K^{-1}$, with a relative standard deviation of more than 100 % ($SD = 9.36 \% K^{-1}$). The 10th and 90th values ranged from 0.71 to $20.22 \% K^{-1}$. The difference of $\Delta RP'_{20}$ among the administrative regions was not significant, varying from 7.21 to $8.40 \% K^{-1}$. NT had the largest median value and largest standard deviation. The median of annual $\Delta RPD'$ was $2.26 \% K^{-1}$ with 10th percentile $-0.31 \% K^{-1}$ and 90th percentile $4.85 \% K^{-1}$. VIC was projected for the largest increase among administrative regions, with up to $3.45 \% K^{-1}$. QLD had the lowest increase value and largest SD, and the largest negative value ($-1.01 \% K^{-1}$) in the 10th percentile projection.

4 Discussion

For climate change impact assessment, results based on an ensemble approach is preferred to a single model run, as a single prediction of future climate made with even the most sophisticated GCM can be of limited use for impact assessment. Within an ensemble approach, provided the members of the ensemble are independent, the ensemble size will have certain effects on the accuracy of the simulation results (Sterl et al., 2007). Hence, one of the main limitations of this research was that both GCM-internal and inter-model ensemble size were rather small: 6 samples for GCM-internal and 12 samples for inter-model ensemble. In addition, the members were assembled on an opportunity basis from available data, rather than designed to sample modelling uncertainties in a systematic way. In our view, therefore, this small sample size was

Applicability of ensemble pattern scaling method

Y. Li and W. Ye

Title Page

Abstract

Introduction

Conclusions

References

Tables

Figures

◀

▶

◀

▶

Back

Close

Full Screen / Esc

Printer-friendly Version

Interactive Discussion



insufficient to reveal the actual relationship between precipitation intensity indices and the global warming trend. In order to get more reliable precipitation change projections especially for extreme precipitation events, more ensemble members are needed including more sample runs from one GCM and more GCMs.

In the GCM-internal ensemble, all the publicly available GCM daily precipitation outputs were used however, this only gave 6 samples. The linearity test of the precipitation intensity indices passed the 95 % significance level for most of the GCMs at the Australian national level, and performed reasonably at the regional level (Tables 1 to 3), which justifies applying the pattern scaling technique in impact assessment studies for precipitation. As expected, the linearity significance became weaker when the spatial/temporal scale got smaller. It is not possible to say, on the basis of this research, how much of this weakness is due to a truly nonlinear response of climate variables to global mean temperature change, and how much is due to the small number in the ensemble size and the short duration of each sample (20 yr). The deteriorating SNR at the grid cell level (Table 4) also casts doubts in applying the pattern scaling method in precipitation intensity analysis, more data are needed in order to investigate the causes for this. The 6 samples of each GCM were from three different emissions scenarios and two 20-yr periods, and the transient climate effect of aerosols on local precipitation patterns (Boer et al., 2000; Menon et al., 2002) can pose another source of the internal variability. More dedicated internal GCM ensemble methods, such as, the perturbed physical ensemble (Murphy et al., 2007) will also need to be explored. Nevertheless, for GCM internal ensembles, the sampling uncertainty arising from the parameterisation of atmospheric physical processes and the effects of natural variability, provide a first opportunity to quantify the robustness of predictions of changes in precipitation obtained from GCM simulations (Barnett et al., 2006). At present, using the average pattern scaling values from all the samples is probably the most appropriate way in constructing the normalised spatial pattern that the pattern scaling method requires.

Applicability of ensemble pattern scaling method

Y. Li and W. Ye

Title Page

Abstract

Introduction

Conclusions

References

Tables

Figures

◀

▶

◀

▶

Back

Close

Full Screen / Esc

Printer-friendly Version

Interactive Discussion



In terms of the GCM inter-model ensemble, the sample size of 12 GCMs used in this study may also be insufficient to reveal the actual distribution of the spectrum of uncertainties caused by different GCM simulations. Furthermore, the inter-model ensemble could be under-dispersive rather than over-dispersive, because the GCM simulations used are not explicitly designed to sample the range of future responses consistent with recent historical observations (Allen and Ingram, 2002). More GCM simulations running under more purposely designed scenarios will be of great help to expose the real uncertainties of future precipitation intensity responses to climate change.

5 Conclusions

Estimating future potential changes in precipitation characteristics provides essential input to urban, regional and national adaptation and planning strategies through the establishment of, for example, flood prevention strategies. This research attempts to highlight and examine the fundamental assumptions of the pattern scaling technique, as well as uncertainty, and contributes to the practical application of GCM-derived climate projections. Through applying a two-step ensemble to 3 precipitation intensity indices, we found that: (1) The accuracy of pattern scaling linearity varies among GCMs and regions. The high linearity can be achieved for most of the GCMs at large spatial scales, such as the national level for Australia. A GCM showing good linearity for one indicator does not guarantee its good linear performance for any other indicator, and the GCM internal signal-to-noise ratios tends to decrease with the spatial scale decline as well. Even though the linearity weakens quickly with increased spatial scale, the error that might be incurred from such GCM internal variability is still much smaller compared to the inter-model variability. Pattern scaling is still a good compromised method in construction of future change of precipitation indices, especially for trend analysis. (2) The two-step ensemble method utilizes all the available information in

Applicability of ensemble pattern scaling method

Y. Li and W. Ye

Title Page

Abstract

Introduction

Conclusions

References

Tables

Figures



Back

Close

Full Screen / Esc

Printer-friendly Version

Interactive Discussion



calculating the scaled response rather than one forcing scenario and/or one GCM, so that the uncertainty level can be directly assessed by statistical analysing of the ensemble results. This study assumed all GCM ensemble members to be equally plausible, with no weighting factor introduced. The two-step ensemble offers an opportunity to evaluate the performance of a given GCM in precipitation simulation, where it is applicable, as a reference for selecting ensemble members. This can assist in selecting appropriate GCMs, or giving sensible weighting factors for selected GCMs in an ensemble. Another advantage of the two step ensemble approach is that it reduces the influence of GCM internal variability. This is particularly important if, in some of the GCM simulation output happens to be at opposite direction of other simulations during the projection periods (Ruosteenoja, et al., 2007). (3) The uncertainties increase when the spatial and/or temporal scales become finer in a given study, which was also found by Tebaldi et al. (2004). Besides obtaining more sample numbers from daily simulations of different GCMs, statistical downscaling or dynamic downscaling might produce more regional information based on the coarse resolution GCM data, and should be more appropriate for regional impact assessments (Wilby et al., 2002; Spak et al., 2007; Haylock et al., 2006; Kennett and Buonomo, 2006). (4) By applying the method to Australia and its administrative regions, we found that, as shown in Table 5, the median value of the annual $\Delta P'_{99}$ was projected to increase by $3.56\% K^{-1}$ for the whole country, with the lowest median increase for QLD ($3.16\% K^{-1}$), and the largest increase for VIC ($6.34\% K^{-1}$). The median value of annual $\Delta RP'_{20}$ over Australia increases $7.62\% K^{-1}$, with a relative standard deviation of more than 100% ($9.36\% K^{-1}$). The 10th and 90th values range from 0.71 to $20.22\% K^{-1}$. The different $\Delta RP'_{20}$ among the administrative regions were not significant, varying from 7.21 to $8.40\% K^{-1}$. The overall average annual $\Delta RPD'$ of 12 GCM ensembles was $2.26\% K^{-1}$ with the 10th and 90th percentiles being -0.31 and $4.85\% K^{-1}$ respectively. Compared to the two extreme precipitation indices, the linear correlation between ΔRPD and ΔT was better. The most extreme index, $\Delta RP'_{20}$ had the lowest number of GCMs which showed significant correlations to ΔT , this indicates the random nature of extreme precipitation.

Applicability of ensemble pattern scaling method

Y. Li and W. Ye

Title Page

Abstract

Introduction

Conclusions

References

Tables

Figures

◀

▶

◀

▶

Back

Close

Full Screen / Esc

Printer-friendly Version

Interactive Discussion



Supplementary material related to this article is available online at:
[http://www.hydrol-earth-syst-sci-discuss.net/8/5227/2011/
hessd-8-5227-2011-supplement.zip](http://www.hydrol-earth-syst-sci-discuss.net/8/5227/2011/hessd-8-5227-2011-supplement.zip).

Acknowledgements. This research is partly supported by the Asia Pacific Network for Global Change Research (APN) CAPaBLE project, CRP2008-02CMY. We acknowledge the modeling groups for making their model output available for analysis; the Program for Climate Model Diagnosis and Intercomparison (PCMDI) for collecting and archiving this data; and the WCRP's Working Group on Coupled Modelling (WGCM) for organizing the model data analysis activity. The WCRP CMIP3 multi-model dataset is supported by the Office of Science, US Department of Energy. L. Storey kindly proofread this manuscript.

References

- Alexander, L. V. and Arblaster, J. M.: Assessing trends in observed and modelled climate extremes over Australia in relation to future projections. *Int. J. Climatol.*, 29, 417–435, doi:10.1002/joc.1730, 2009.
- Allen, M. R. and Ingram, W. J.: Constraints on future changes in climate and the hydrologic cycle. *Nat.*, 419, 224–232, 2002.
- Barnett, D. N., Brown, S. J., Murphy, J. M., Sexton, D. M. H., and Webb, M. J.: Quantifying uncertainty in changes in extreme event frequency in response to doubled CO₂ using a large ensemble of GCM simulations, *Clim. Dyn.*, 26, 489–511, doi:10.1007/s00382-005-0097-1, 2006.
- Boer, G. J., Flato, G., and Ramsden, D.: A transient climate change simulation with greenhouse gas and aerosol forcing: projected climate to the twenty-21st century, *Clim. Dyn.*, 16, 427–450, 2000.
- Chernick, M. R.: *Bootstrap Methods, A practitioner's guide*, Wiley Series in Probability and Statistics, 1999.
- CSIRO: Climate Change in Australia – Technical Report, available at: <http://climatechangeinaustralia.com.au/resources.php>, last access: 25 May 2011, 2007.
- Dai, A.: Precipitation characteristics in eighteen coupled climate models, *J. Clim.*, 19, 4605–4630, 2006.

Applicability of ensemble pattern scaling method

Y. Li and W. Ye

Title Page

Abstract

Introduction

Conclusions

References

Tables

Figures

◀

▶

◀

▶

Back

Close

Full Screen / Esc

Printer-friendly Version

Interactive Discussion



Applicability of ensemble pattern scaling method

Y. Li and W. Ye

Title Page

Abstract

Introduction

Conclusions

References

Tables

Figures

◀

▶

◀

▶

Back

Close

Full Screen / Esc

Printer-friendly Version

Interactive Discussion



- Furrer, R., Sain, S. R., Nychka, D., and Meehl, G. A.: Multivariate Bayesian analysis of atmosphere–ocean general circulation models, *Environ. and Ecol. Stat.*, 14, 249–266, doi:10.1007/s10651-007-0018-z, 2007.
- Giorgi, F. and Mearns, L.: Probability of regional climate change calculated using the reliability ensemble average (REA) method, *Geophys. Res. Lett.*, 30, 1629–1632, doi:10.1029/2003GL017130, 2003.
- Good, P., Barring, L., Giannakopoulos, C., Holt, T., and Palutikof, J.: Non-linear regional relationships between climate extremes and annual mean temperatures in model projections for 1961–2099 over Europe, *Clim. Res.*, 31, 19–34, doi:10.3354/cr031019, 2006.
- Haylock, M. R., Cawley, G. C., Harpham, C., Wilby, R. L., and Goodess, C. M.: Down-scaling heavy precipitation over the United Kingdom: A comparison of dynamical and statistical methods and their future scenarios, *Int. J. Climatol.*, 26(10), 1397–1415, doi:10.1002/joc.1318, 2006.
- Kennett, E. J. and Buonomo, E.: Methodologies of pattern scaling across the full range of RT2A GCM ensemble members, available at: http://ensembles-eu.metoffice.com/project_reporting/year2reporting/public_completed_milestones_deliverables_13_24/D2B.7_pattern_scaling.pdf, last access: 25 May 2011, 2006.
- Kharin, V. V., Zwiers, F. W., Zhang, X., and Hegerl, G. C.: Changes in temperature and precipitation extremes in the IPCC ensemble of global coupled model simulations, *J. Clim.*, 20(8), 1419–1444, doi:10.1175/JCLI4066.1, 2007.
- Kiktev, D., Caesar, J., Alexander, L. V., Shiogama, H., and Collier, M.: Comparison of observed and multi-model trends in annual extremes of temperature and precipitation, *Geophys. Res. Lett.*, 34, L10702, doi:10.1029/2007GL029539, 2007.
- Li, Y., Ye, W., Wang, M., and Yan, X.: Climate change and drought: a risk assessment of crop yield impacts, *Clim. Res.*, 39(1), 31–46, doi:10.3354/cr00797, 2009.
- Meehl, G. A., Stocker, T. F., Collins, W. D., Friedlingstein, P., Gaye, A. T., Gregory, J. M., Kitoh, A., Knutti, R., Murphy, J. M., Noda, A., Raper, S. C. B., Watterson, I. G., Weaver, A. J., and Zhao, Z.: Global climate projections, in: *Climate Change 2007: The physical science basis. Contribution of working group I to the fourth assessment report of the Intergovernmental Panel on Climate Change*, edited by: Solomon, S., Qin, D., Manning, M., Chen, Z., Marquis, M., Averyt, K. B., Tignor, M., and Miller, H. L., Cambridge, UK and New York, NY: Cambridge University Press, 2007.
- Menon, S., Hansen, J., Nazarenko, L., and Luo, Y.: Climate effects of black carbon aerosols in

Applicability of ensemble pattern scaling method

Y. Li and W. Ye

Title Page

Abstract

Introduction

Conclusions

References

Tables

Figures

◀

▶

◀

▶

Back

Close

Full Screen / Esc

Printer-friendly Version

Interactive Discussion



China and India, *Science*, 297, 2250–2252, 2002.

Min, S., Simonis, D., and Hense, A.: Probabilistic climate change predictions applying Bayesian model averaging, *Phil. Trans. R. Soc. A*, 365, 2103–2116, doi:10.1098/rsta.2007.2070, 2007.

5 Mitchell, T. D.: Pattern scaling: An examination of the accuracy of the technique for describing future climates, *Climatic Change*, 60, 217–242, 2003.

Moise, A. F. and Hudson, D. A.: Probabilistic predictions of climate change for Australia and southern Africa using the reliability ensemble average of IPCC CMIP3 model simulations, *J. Geophys Res.*, 113, D15113, doi:10.1029/2007JD009250, 2008.

10 Murphy, J. M., Sexton, D. M., Barnett, D. N., Jones, G. S., Webb, M. J., Collins, M., and Stainforth, D. A.: Quantification of modelling uncertainties in a large ensemble of climate change simulations, *Nature*, 430(7001), 768–772, doi:10.1038/nature02771, 2004.

Murphy, J. M., Booth, B. B. B., Collins, M., Harris, G. R., Sexton, D. M. H., and Webb, M. J.: A methodology for probabilistic predictions of regional climate change from perturbed physics ensembles, *Phil. T. R. Soc. A*, 365, 1993–2028, doi:10.1098/rsta.2007.2077, 2007.

15 Parzen E.: On estimation of a probability density function and mode, *Ann. Math. Stat.*, 33, 1065–1076, 1962.

Perkins, S. E., Pitman, A. J., Holbrook, N. J., and McAneney, J.: Evaluation of the AR4 climate models' simulated daily maximum temperature, minimum temperature, and precipitation over Australia using probability density functions, *J. Clim.*, 20(17), 4356–4376, doi:10.1175/JCLI4253.1, 2007.

20 Räisänen, J.: How reliable are climate models?, *Tellus A*, 59(1), 2–29, doi:10.1111/j.1600-0870.2006.00211.x, 2007.

Räisänen, J. and Palmer, T. N.: A probability and decision-model analysis of a multi-model ensemble of climate change simulations, *J. Clim.*, 14, 3212–3226, 2001.

25 Raper, S. C. B., Gregory, J. M., and Osborn, T. J.: Use of an upwelling-diffusion energy balance climate model to simulate and diagnose A/OGCM results, *Clim. Dyn.*, 17, 601–613, 2001.

Ruosteenoja, K., Tuomenvirta, H., and Jylhä, K.: GCM-based regional temperature and precipitation change estimates for Europe under four SRES scenarios applying a super-ensemble pattern-scaling method, *Climat. Chang.*, 81, 193–208, doi:10.1007/s10584-006-9222-3, 2007.

30 Santer, B. D., Wigley, T. M. L., Schlesinger, M. E., and Mitchell, J. F. B.: Developing climate scenarios from equilibrium GCM results, MPI Report Number 47, Hamburg, 1990.

Applicability of ensemble pattern scaling method

Y. Li and W. Ye

Title Page

Abstract

Introduction

Conclusions

References

Tables

Figures

◀

▶

◀

▶

Back

Close

Full Screen / Esc

Printer-friendly Version

Interactive Discussion

- Shi, G., Cai, W., Cowan, T., Ribbe, J., Rotdtayn, L., and Dix, M.: Variability and trend of north west Australia rainfall: Observations and coupled climate modeling, *J. Clim.*, 21(12), 2938–2959, doi:10.1175/2007JCLI1908.1, 2008.
- Sorteberg, A. and Kvamsto, N. G.: The effect of internal variability on anthropogenic climate projections, *Tellus*, 58A, 565–574, doi:10.1111/j.1600-0870.2006.00202.x, 2006.
- Spak, S., Holloway, T., Lynn, B., and Goldberg, R.: A comparison of statistical and dynamical downscaling for surface temperature in North America, *J. Geophys. Res.*, 112, D08101, doi:10.1029/2005JD006712, 2007.
- Sterl, A., Severijns, C., Van, Oldenborgh, G. J., Dijkstra, H., Hazeleger, W., Van den Broeke, M., Burgers, G., Van den Hurk, B., Van Leeuwen, P. J., and Van Velthoven, P.: The ESSENCE project – signal to noise ratio in climate projections, available at: http://www.knmi.nl/\simster/Essence/essence_1.v2.2.pdf, 2007.
- Task Group on Data and Scenario Support for Impact and Climate Assessment (TGICA) Intergovernmental Panel on Climate Change: General guidelines on the use of scenario data for climate impact and adaptation assessment, Version 2, 2007.
- Tebaldi, C. and Knutti, R.: The use of the multi-model ensemble in probabilistic climate projections, *Phil. T. R. Soc. A*, 365, 2053–2075, doi:10.1098/rsta.2007.2076, 2007.
- Tebaldi, C., Nychka, D., and Mearns, L. O.: From global mean responses to regional signals of climate change: simple pattern scaling, its limitations (or lack of) and the uncertainty in its results. In *Proceedings of the 18th Conference on Probability and Statistics in the Atmospheric Sciences*, AMS Annual Meeting, Seattle, WA, 2004.
- Tebaldi, C., Smith, R., Nychka, D., and Mearns, L.: Quantifying uncertainty in projections of regional climate change: a Bayesian approach to the analysis of multi-model ensembles, *J. Clim.*, 18, 1524–1540, doi:10.1175/JCLI3363.1, 2005.
- Tebaldi, C., Hayhoe, K., Arblaster, J. M., and Meehl, G. A.: Going to the extremes: an intercomparison of model-simulated historical and future changes in extreme events, *Clim. Chang.*, 79, 185–211, doi:10.1007/s10584-006-9051-4, 2006.
- Whetton, P.: Methods used to prepare the ranges of projected future change in Australian region temperature and precipitation (<http://www.dar.csiro.au/impacts/docs/how.pdf>), 2001.
- Wilby, R. L., Dawson, C. W., and Barrow, E. M.: SDSM – A decision support tool for the assessment of regional climate change impacts, *Environ. Model. Softw.*, 17, 147–159, 2002.

Table 1. GCM internal ensemble of ΔP_{99} in response to ΔT and the signal-to-noise ratio (SNR) of 6 simulation samples over Australia.

	NSW			NT			QLD			SA		
	R^2	ΔP_{99}	SNR	R^2	ΔP_{99}	SNR	R^2	ΔP_{99}	SNR	R^2	ΔP_{99}	SNR
1	0.27	3.45	0.81	0.43	3.73	0.87	0.30	2.67	0.69	0.59	2.63	0.76
2	0.43	2.36	0.42	0.63	16.42	3.13	0.30	4.32	0.68	0.79*	3.20	1.51
3	0.08	3.18	0.93	0.70*	5.93	6.11	0.60	7.48	3.74	0.77*	6.39	3.97
4	0.67*	6.62	2.96	0.55	8.58	3.61	0.70*	5.87	4.22	0.26	5.82	1.05
5	0.84*	9.05	6.61	0.12	8.03	2.29	0.17	6.91	2.27	0.38	10.86	3.08
6	0.83*	6.09	6.48	0.54	3.52	2.50	0.63	3.03	3.94	0.95*	4.91	3.51
7	0.67*	2.20	0.60	0.96*	24.72	12.30	0.43	16.38	3.94	0.01	8.09	1.22
8	0.01	0.86	0.20	0.63	15.11	2.96	0.38	9.87	1.70	0.93*	0.80	0.14
9	0.36	7.95	1.52	0.73*	8.96	3.64	0.73*	15.11	2.31	0.26	7.79	1.77
10	0.75*	5.15	3.03	0.53	2.40	2.50	0.83*	2.06	1.72	0.25	5.23	2.11
11	0.07	2.62	0.87	0.01	-1.17	0.25	0.12	0.00	0.00	0.19	4.52	0.69
12	0.18	0.28	0.28	0.09	-0.44	0.49	0.00	1.10	1.62	0.12	-0.53	0.26

	TAS			VIC			WA			AUS		
	R^2	ΔP_{99}	SNR									
1	0.09	2.49	0.40	0.60	3.39	0.99	0.15	0.66	0.10	0.30	2.42	0.52
2	0.83*	10.66	4.28	0.87*	9.14	1.89	0.08	11.19	2.68	0.97*	8.53	10.80
3	0.99*	1.41	0.56	0.24	9.49	2.41	0.72*	6.43	3.44	0.91*	6.56	8.41
4	0.08	-0.33	0.16	0.24	5.38	0.91	0.01	3.27	1.19	0.62	5.19	4.19
5	0.79*	9.08	4.86	0.53	9.62	3.46	0.82*	7.89	5.40	0.72*	8.01	5.17
6	0.76*	6.03	3.37	0.72*	8.86	5.47	0.33	2.42	2.24	0.86*	4.05	6.33
7	0.07	17.55	2.01	0.53	8.59	1.49	0.36	12.65	3.37	0.89*	13.77	8.50
8	0.03	8.45	0.89	0.01	7.29	1.30	0.94*	13.98	5.55	0.79*	10.07	5.22
9	0.30	0.81	0.68	0.77*	1.79	0.82	0.85*	10.46	5.45	0.79*	9.67	3.66
10	0.56	7.41	3.38	0.62	10.12	4.27	0.07	2.35	2.10	0.69*	3.67	4.42
11	0.23	7.81	2.06	0.71*	6.83	1.35	0.01	1.94	1.18	0.12	3.06	1.39
12	0.92*	2.00	1.80	0.78*	1.79	2.01	0.00	1.10	1.69	0.22	0.82	1.71

* The confidence level is over 95%.

Applicability of ensemble pattern scaling method

Y. Li and W. Ye

Title Page

Abstract Introduction

Conclusions References

Tables Figures

◀ ▶

◀ ▶

Back Close

Full Screen / Esc

Printer-friendly Version

Interactive Discussion



Table 2. GCM internal ensemble ΔRP_{20} in response to ΔT and the signal-to-noise ratio (SNR) of 6 simulation samples over Australia.

	NSW			NT			QLD			SA		
	R^2	$\Delta RP'_{20}$	SNR									
1	0.26	7.61	1.71	0.01	4.15	1.25	0.46	8.06	2.92	0.12	4.52	2.35
2	0.71*	8.62	1.05	0.43	24.90	2.68	0.81*	12.49	2.79	0.78*	7.72	1.34
3	0.13	8.06	1.14	0.14	10.76	2.61	0.46	8.43	2.98	0.44	8.23	2.24
4	0.41	5.70	2.02	0.31	5.98	3.02	0.61	4.83	2.65	0.12	1.17	0.24
5	0.60	11.10	4.01	0.24	9.61	2.36	0.52	10.67	3.84	0.49	13.39	3.16
6	0.91*	7.06	3.41	0.49	6.84	2.21	0.61	5.29	2.37	0.86*	9.48	2.36
7	0.94*	3.97	0.89	0.93*	36.87	6.22	0.78*	22.47	4.09	0.41	12.41	2.27
8	0.12	4.39	0.88	0.97*	28.39	3.96	0.49	15.52	1.50	0.87*	1.43	0.24
9	0.51	9.29	1.41	0.77*	17.33	2.76	0.56	20.27	1.90	0.46	8.63	1.72
10	0.74*	6.53	3.93	0.00	1.54	0.47	0.09	5.92	1.80	0.09	9.64	2.37
11	0.27	5.95	0.86	0.25	3.85	0.59	0.40	4.53	0.96	0.12	8.37	1.02
12	0.08	1.55	0.39	0.39	0.97	0.27	0.06	2.23	0.58	0.05	0.08	0.02
	TAS			VIC			WA			AUS		
	R^2	$\Delta RP'_{20}$	SNR									
1	0.33	7.36	1.47	0.22	7.13	1.57	0.56	4.51	1.73	0.41	5.60	2.96
2	0.83*	2.76	0.53	0.92*	8.16	0.94	0.41	21.81	3.27	0.75*	15.22	3.30
3	0.20	3.54	0.86	0.07	8.16	1.19	0.15	9.55	2.87	0.32	8.52	2.65
4	0.00	-2.12	0.36	0.17	1.33	0.17	0.13	1.27	0.46	0.35	2.79	2.13
5	0.10	16.24	2.27	0.83*	10.11	5.32	0.92*	11.35	6.84	0.79*	10.31	6.53
6	0.93*	5.40	2.35	0.67*	11.55	3.25	0.68*	4.07	1.65	0.84*	6.52	3.23
7	0.32	18.02	2.62	0.68*	10.80	1.84	0.60	16.97	2.28	0.86*	20.46	4.57
8	0.07	9.34	1.00	0.21	8.61	2.54	0.90*	20.81	5.48	0.83*	16.35	4.19
9	0.67*	4.57	2.33	0.58	-0.23	0.06	0.88*	16.41	3.95	0.73*	14.16	2.45
10	0.16	8.35	2.33	0.49	8.13	3.00	0.00	3.32	1.48	0.12	4.90	2.40
11	0.01	14.55	1.13	0.61	9.84	1.58	0.51	6.96	2.07	0.44	6.94	1.47
12	0.44	12.18	2.46	0.81*	4.63	1.27	0.19	2.08	0.55	0.04	2.21	0.64

* The confidence level is over 95%.

Applicability of ensemble pattern scaling method

Y. Li and W. Ye

Title Page

Abstract

Introduction

Conclusions

References

Tables

Figures

◀

▶

◀

▶

Back

Close

Full Screen / Esc

Printer-friendly Version

Interactive Discussion



Applicability of ensemble pattern scaling method

Y. Li and W. Ye

Table 4. The grid cell percentages at different SNR levels for 12 GCMs and 3 precipitation intensity indices.

	$\Delta P'_{99}$			$\Delta RP'_{20}$			$\Delta RPD'$		
	> 0.5	> 1.0	> 2.0	> 0.5	> 1.0	> 2.0	> 0.5	> 1.0	> 2.0
BCCR_BCM20	51.64	10.78	1.09	86.4	42.27	7.16	85.31	57.72	15.42
CCCMA_CGCM3	74.88	53.58	13.66	95.57	65.06	25.86	92.35	69.10	19.91
CNRM_CM3	89.22	63.7	8.00	94.06	59.51	15.28	88.66	63.90	18.25
CSIRO_MK35	81.05	46.03	13.28	77.53	37.70	5.43	79.21	37.59	5.71
MPI_ECHAM5	95.72	78.67	24.23	93.42	76.08	31.89	99.55	96.14	65.37
ECHO_G	88.08	67.88	24.19	93.78	74.07	23.03	98.66	95.57	71.74
GFDL_CM20	89.37	54.10	16.95	88.67	68.65	25.71	79.39	45.11	8.07
GFDL_CM21	76.17	37.17	9.35	82.30	59.77	22.47	73.28	36.79	7.68
IPSL_CM40	85.85	52.14	11.04	95.38	71.77	17.65	76.54	49.60	11.93
MIROC_MEDRES	87.63	58.63	25.44	80.72	52.34	14.16	95.23	85.52	50.45
MRI_CGCM2	64.73	28.54	5.49	82.75	36.40	3.15	56.56	12.76	2.22
NCAR_CCSM3	82.11	40.8	5.55	77.09	39.79	8.40	97.7	89.74	55.26
Average	80.54	49.34	13.19	87.31	56.95	16.68	85.20	61.63	27.67

Title Page

Abstract Introduction

Conclusions References

Tables Figures

◀ ▶

◀ ▶

Back Close

Full Screen / Esc

Printer-friendly Version

Interactive Discussion



Applicability of ensemble pattern scaling method

Y. Li and W. Ye

Title Page

Abstract

Introduction

Conclusions

References

Tables

Figures

◀

▶

◀

▶

Back

Close

Full Screen / Esc

Printer-friendly Version

Interactive Discussion



Table 5. The inter- model ensemble results of 3 precipitation intensity indices.

		NSW	NT	QLD	SA	TAS	VIC	WA	AUS
$\Delta P'_{99}$	Median	3.23	4.09	3.16	3.64	4.09	6.34	3.33	3.56
	SD	5.07	9.57	7.49	5.66	5.16	4.10	7.60	7.23
	10th	-1.40	-0.02	-0.24	-0.97	0.81	1.48	-0.71	-0.52
	90th	9.78	17.26	14.90	11.20	11.12	11.12	14.71	14.01
$\Delta RP'_{20}$	Median	7.21	8.40	7.72	7.19	7.36	7.94	7.45	7.62
	SD	4.67	14.4	9.5	6.72	6.21	5.07	9.89	9.36
	10th	0.86	0.98	1.77	-0.16	2.63	0.59	0.14	0.71
	90th	11.55	27.88	21.05	14.38	16.54	12.3	21.96	20.22
$\Delta RPD'$	Median	2.55	2.23	1.83	2.82	1.91	3.45	2.12	2.26
	SD	1.94	2.51	2.79	2.39	1.73	1.94	2.35	2.41
	10th	0.52	-0.46	-1.01	0.53	-0.36	1.06	-0.55	-0.32
	90th	4.79	5.05	4.73	5.78	3.47	5.61	4.42	4.85

Applicability of ensemble pattern scaling method

Y. Li and W. Ye

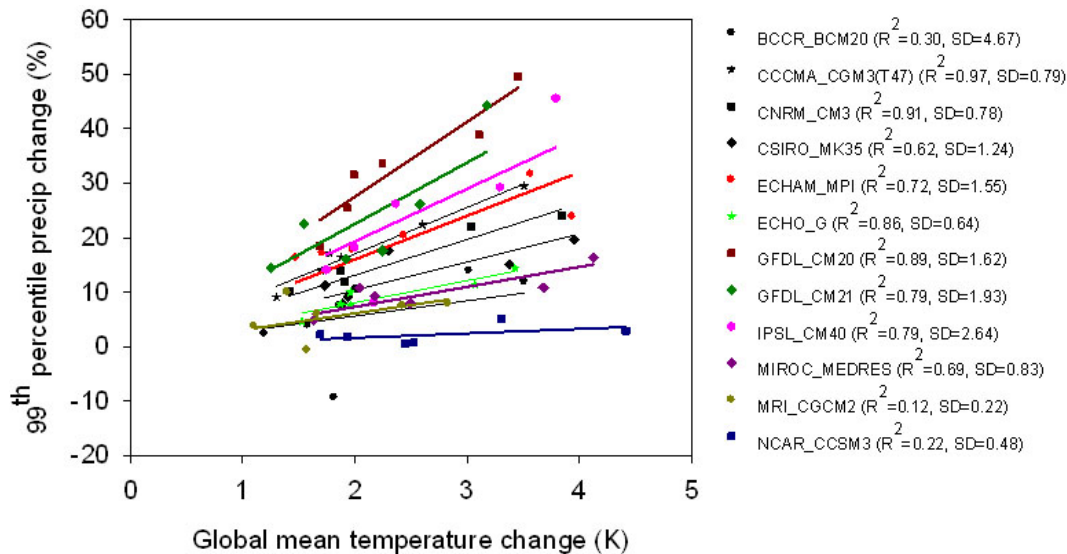


Fig. 1. The linearity of annual ΔP_{99} in response to global mean temperature change for Australia.

Title Page

Abstract

Introduction

Conclusions

References

Tables

Figures

◀

▶

◀

▶

Back

Close

Full Screen / Esc

Printer-friendly Version

Interactive Discussion



Applicability of ensemble pattern scaling method

Y. Li and W. Ye

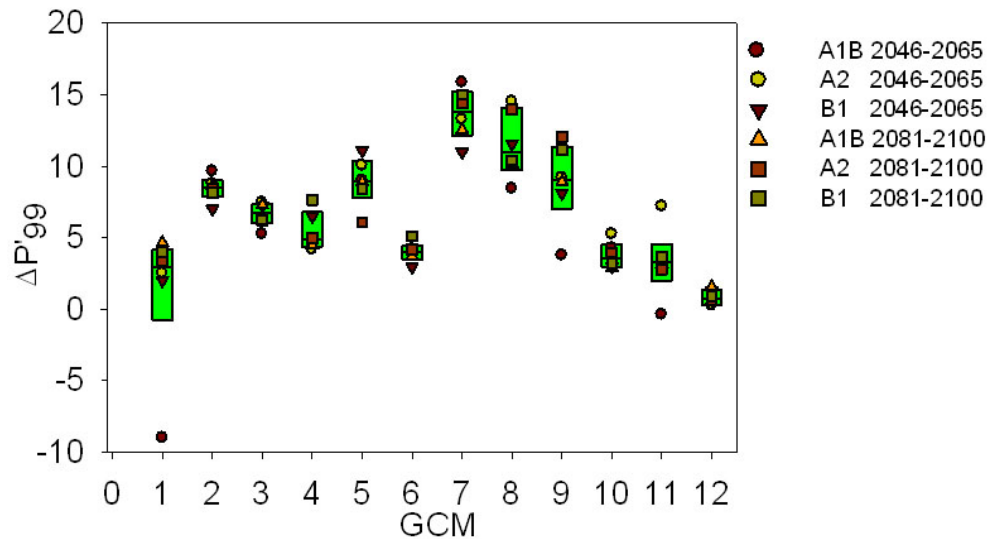


Fig. 2. The internal and inter-model variability in annual $\Delta P'_{99}$ overall Australia. Shade-boxes are the median, 5th and 95th percentile.

Discussion Paper | Discussion Paper | Discussion Paper | Discussion Paper | Discussion Paper

Title Page

Abstract

Introduction

Conclusions

References

Tables

Figures

◀

▶

◀

▶

Back

Close

Full Screen / Esc

Printer-friendly Version

Interactive Discussion



Applicability of ensemble pattern scaling method

Y. Li and W. Ye

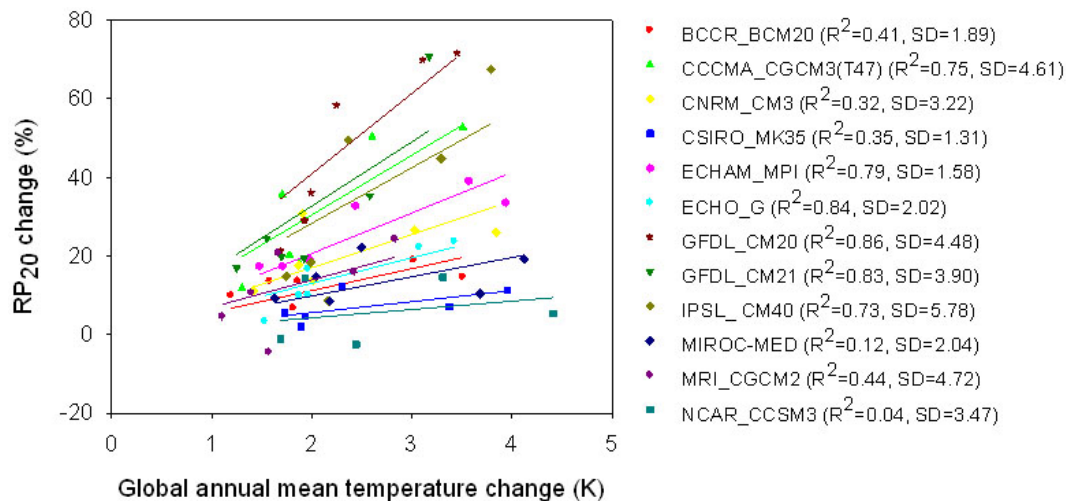


Fig. 3. The linearity of annual ΔRP_{20} in response to global mean temperature change in Australia.

Title Page

Abstract

Introduction

Conclusions

References

Tables

Figures

◀

▶

◀

▶

Back

Close

Full Screen / Esc

Printer-friendly Version

Interactive Discussion



Applicability of ensemble pattern scaling method

Y. Li and W. Ye

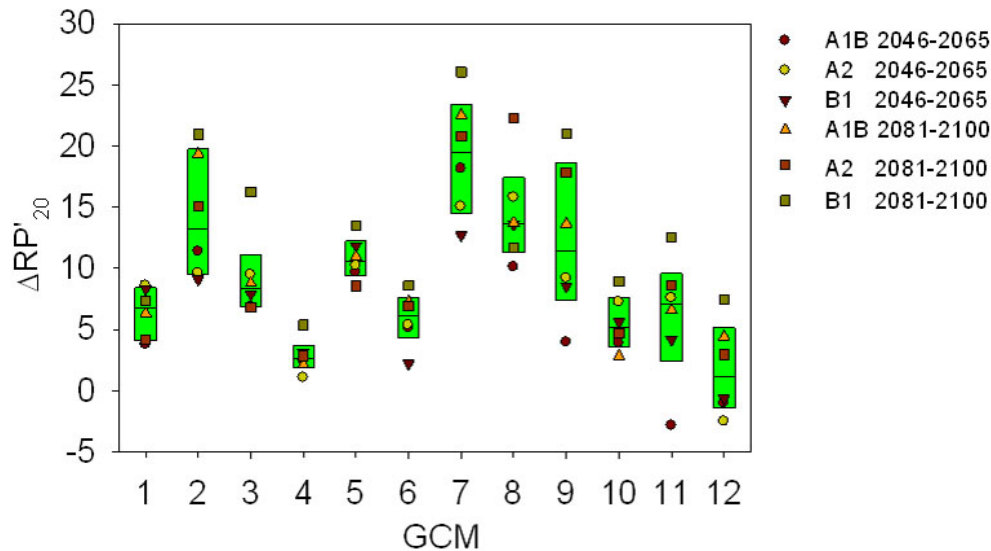


Fig. 4. The internal and inter-model variability in annual and seasonal $\Delta RP'_{20}$ over Australia. Shade- boxes are the median, the 5th and 95th percentiles.

Discussion Paper | Discussion Paper | Discussion Paper | Discussion Paper | Discussion Paper

Title Page

Abstract

Introduction

Conclusions

References

Tables

Figures

◀

▶

◀

▶

Back

Close

Full Screen / Esc

Printer-friendly Version

Interactive Discussion



Applicability of ensemble pattern scaling method

Y. Li and W. Ye

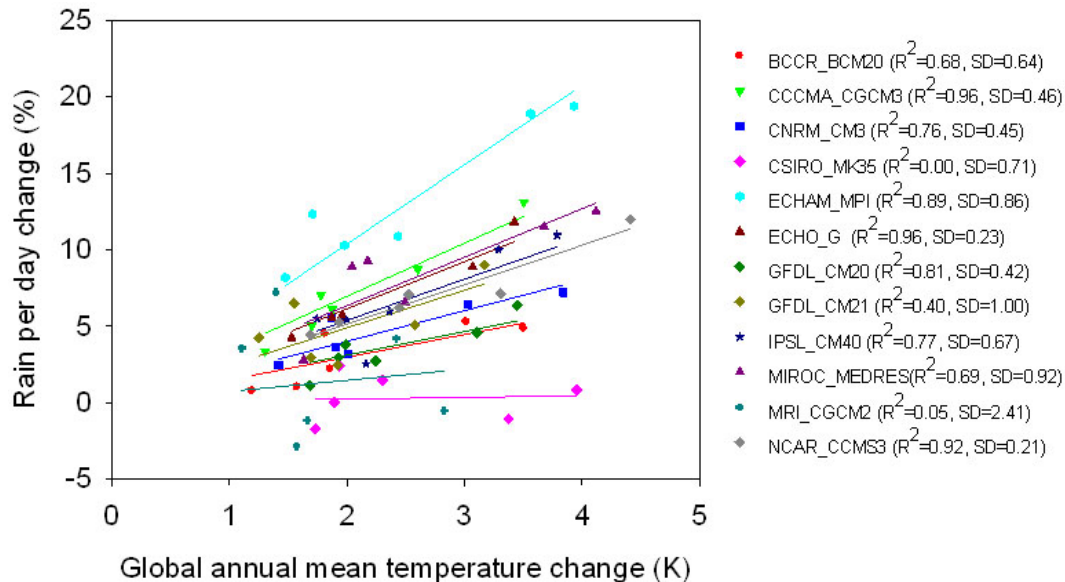


Fig. 5. The linearity of annual Δ RPD in responses to global annual mean temperature change in Australia.

Title Page

Abstract

Introduction

Conclusions

References

Tables

Figures

◀

▶

◀

▶

Back

Close

Full Screen / Esc

Printer-friendly Version

Interactive Discussion



Applicability of ensemble pattern scaling method

Y. Li and W. Ye

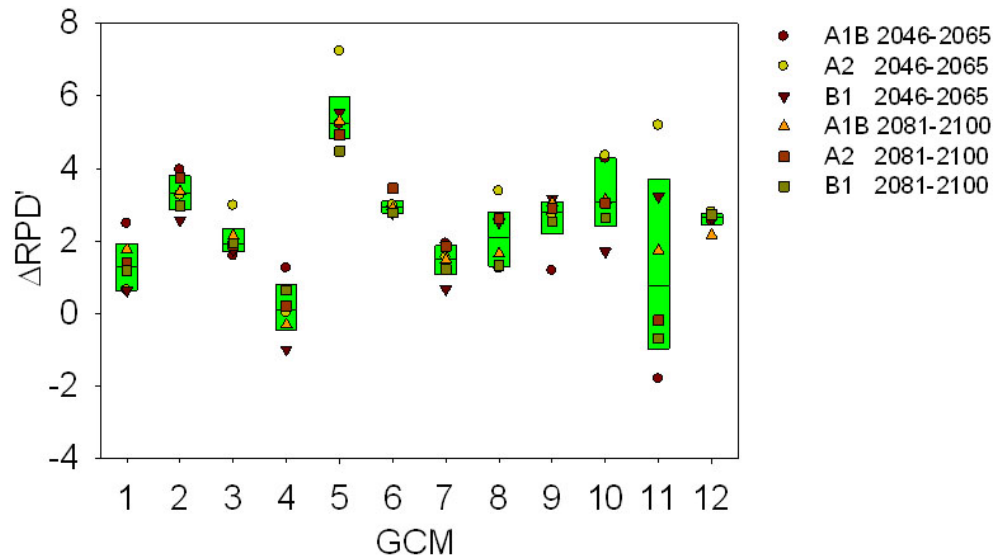


Fig. 6. The internal and inter-model variability in annual $\Delta RPD'$ over Australia. The boxes are the median, 5th and 95th percentile.

Discussion Paper | Discussion Paper | Discussion Paper | Discussion Paper | Discussion Paper

Title Page

Abstract Introduction

Conclusions References

Tables Figures

◀ ▶

◀ ▶

Back Close

Full Screen / Esc

Printer-friendly Version

Interactive Discussion



Applicability of ensemble pattern scaling method

Y. Li and W. Ye

Title Page

Abstract

Introduction

Conclusions

References

Tables

Figures

◀

▶

◀

▶

Back

Close

Full Screen / Esc

Printer-friendly Version

Interactive Discussion

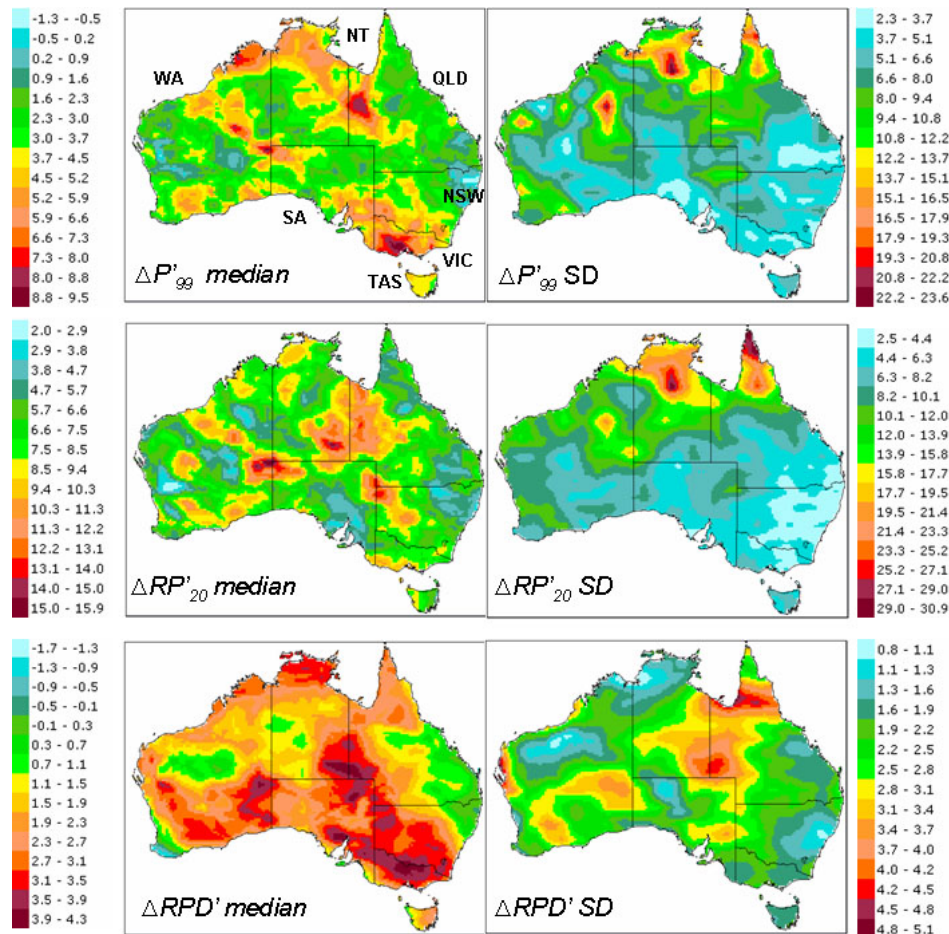


Fig. 7. The comparison of inter-model ensemble annual median values ($\%/K^{-1}$) and standard deviations of change patterns for the three precipitation intensity indicators.